IRAQI JOURNAL OF APPLIED PHYSICS
Vol. 22, No. 4, October-December 2026, pp. 611-616

Optical and Structural Properties of Tin Dioxide Thin Films Prepared by Pulsed-Laser Deposition for High-Efficiency Solar Cells

Sawsan H. Abdullah [1*]
Hala A. Abed [2]
Aysar J. Hamad [3]
Karameh A. Muhammad [1]

[1] Ministry of Higher Education and Scientific Research, Scientific Research Commission, Baghdad, IRAQ
[2] Department of Atmospheric Science, College of Science, Mustansiriyah University, Baghdad, IRAQ
[3] College of Pharmacy, Al-Farabi University, Baghdad, IRAQ
* Corresponding author email: sawsanhussein1976@gmail.com

Thin films of SnO_2 deposited by the pulsed-laser deposition (PLD) method using high-purity SnO_2 powder as the target. The deposition was done at room temperature and the film thickness was ≈200 nm. Laser-induced breakdown spectroscopy (LIBS) confirmed the pure state of the target material and the characteristic tin emission lines were observed with no visible impurities. The films deposited on the platform have a highly crystalline tetragonal rutile SnO_2 phase and crystallite sizes between 26.7 and 46.5 nm. The film surface was smooth and homogeneous, a roughness of the RMS was found to be 3.64 nm, and grains were approximately 64.06 nm. The optical bandgap was about 3.4 eV. The developed SnO_2/porous silicon (PSi) solar cell exhibited a short-circuit current density of 29 mA/cm², open-circuit voltage of 0.4 V, fill factor of 32.5%, and overall conversion efficiency of 3.77%.

Keywords: Tin dioxide; Thin films; Pulsed-laser deposition; Solar cells
Received: 10 November 2025; Revised: 2 February 2026; Accepted: 9 February 2026; Published: 1 October 2026

1. Introduction

Pulsed-laser deposition (PLD) is an innovative method for the generation of thin films with precise control over the fundamental properties of materials [1,2]. The technique is based on the ablation of solid targets by high-energy laser pulses, followed by the formation of a plasma plume which deposits onto a substrate [3-5]. Key benefits of this technique are maintained target material stoichiometry, high film purity, and excellent film thickness and uniformity control. Additionally, PLD is considered an environmentally friendly process [6,7]. Tin oxide (SnO_2) is a typical n-type wide bandgap semiconductor and has a series of advantages in optical, electrical, and chemical properties, making it of interest for applications as solar cells, gas sensors, and transparent conductive electrodes [8]. Owing to the superior optical transparency in the visible region as well as higher thermal stability and conductivity, its utilization as a transparent electrode causes enhancement in optoelectronic devices [9]. For solar cells, SnO_2 is important to enhance light absorption, charge carrier transport, and efficiency [10]. Porous silicon (PSi) has been widely explored as a photovoltaic (PV) substrate with light-trapping capability and a high surface-to-volume ratio that can improve photon absorption, hence the effective junction area [11]. Thus, the incorporation of SnO_2 thin films in PSi substrates is an important purposeful heterojunction design, in which the wide-bandgap, highly transparent SnO_2 layer acts as a window and interfacial layer while the PSi substrate provides the light harvesting and interfacial charge separation. Here, we report on the deposition of high-purity SnO_2 thin films by the PLD method and conduct an investigation of the optical, structural, and photovoltaic characteristics of the films. In this paper, utilizing the SnO_2 films integrated with porous silicon, we seek to evaluate and characterize SnO_2 as a transparent conductive and interfacial layer in solar cell applications.

2. Experimental Part

In order to verify the purity of the SnO_2 powder used as the PLD target, the LIBS analysis was performed. A pulse of Nd:YAG laser beam was focused onto the SnO_2 powder surface, and a plasma plume was created. Thin films of pure SnO_2 were deposited with the PLD process inside a cylindrical vacuum chamber under high vacuum using a working pressure of 2.5×10^{-2} mbar. An Nd:YAG laser beam was incident through a glass window at an angle of 45° onto the target surface. The substrate was oriented horizontally beneath the center of the target at a target–substrate distance of approximately 5 cm, ensuring that the substrate holder did not obstruct the laser beam path.

The glass substrates (7.5×2.5 cm²) were cleaned in an ultrasonic bath first with alcohol and then with distilled water for 15 minutes, respectively, and dried. The target was pure SnO_2 powder (99.99% purity), which was crushed in a planetary mill for homogenization and then pressed with a high-pressure hydraulic press with a pressure of 6 MPa for 10 min to form round pellets of 20 mm diameter and 15 mm thickness. Figure (1) depicts a schematic diagram of the main steps of the PLD process of a laser beam incident on the SnO_2 target, formation of a plasma plume, and thin film deposition on the surface.

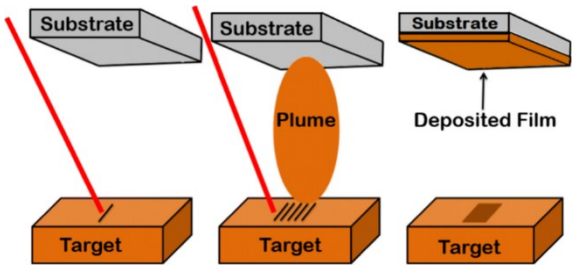

Fig. (1) Schematic diagram of the PLD process

This was used to compose porous silicon and SnO_2 thin films by PLD for solar cell fabrication. To increase the surface area and the light-trapping ability, porous silicon was initially fabricated using the photoelectrochemical etching (PECE) method. Then, SnO_2 thin films were grown at vacuum pressure of 2.5×10^{-2} mbar by 1064 nm Nd:YAG laser. The solar cells benefit from SnO_2 for its high transparency and consequent conductivity, with light absorption and charge transport improvement. They evaporated aluminum on the top sides and the bottom to add conductivity to complete the device. The solar cells used a p-n junction constructed at the boundary between porous silicon (PSi) and SnO_2, which allows the conversion of sunlight into electrical energy through the photovoltaic effect. Dark and illuminated I-V curves were used to evaluate device performance, and overall efficiency (η) was calculated as follows [12]:

$$\eta = \frac{P_m}{P_{in}} = \frac{FF.I_{SC}.V_{OC}}{P_{in}} \times 100\% \quad (1)$$

where FF is the fill factor, which represents the ratio of maximum power to the product of current and voltage at maximum points

Various techniques were used to find the thickness, structural, morphological, and optical properties of the films. Thickness was determined with the optical interferometer method according to light interferences reflected from the surface of the film and the cavity is formed between the air gap of the substrate and the waves between the substrate top surface and the substrate bottom He-Ne laser (632.8 nm), thickness was computed from [13]:

$$t = \frac{\Delta X}{X} \cdot \frac{\lambda}{2} \quad (2)$$

where ΔX is the path fringe displacement, X is a fringe manner, and λ is the wavelength of laser light

Surface morphology and roughness were studied using an atomic force microscope (AFM) in non-contact mode, generates interactions that take place between a nanoscale tip and the surface of the sample and generates 3D topographical images. For structural analysis, X-ray diffraction (XRD) was carried out using a Bruker D2 PHASER instrument with Cu-Kα radiation (λ=1.54056Å). The crystallite size was computed via the Scherrer's equation [14]:

$$D = \frac{k\lambda}{\beta cos\theta} \quad (3)$$

where D is the crystallite size, B is the full-width at half maximum (FWHM), and θ is the Bragg's diffraction angle

The strain (ε) is calculated by the following equation [15]:

$$\varepsilon = \frac{d_{exp.} - d_{std.}}{d_{std.}} \quad (4)$$

A UV–Visible–NIR spectrophotometer was employed to study the optical properties in the 200–1100 nm range. Absorbance (A) was computed by the equation [16]:

$$A = -log_{10}\left(\frac{I}{I_0}\right) \quad (5)$$

where I_0 is the incident light intensity and I is the transmitted light

Tauc's relation was used to calculate the optical bandgap (E_g) as [17]:

$$(\alpha hv)^n = A(hv - E_g) \quad (6)$$

where hν is the photon energy, A is a constant, and n is dependent upon the type of electronic transition (n=2 for direct transitions and n=1/2 for indirect transitions) [18]. The value of the bandgap (E_g) was calculated by plotting $(\alpha hv)^2$ versus hv and extrapolating the straight part to intersect the hv-axis.

3. Results and Discussion

A LIBS analysis was performed to validate the purity of the tin oxide powder used as the target material. The emission spectra recorded are depicted in Fig. (2). It is obvious from the spectral lines that the major characteristics of the star spectra belong to neutral and singly ionized tin species. The evident lines include the following features: Sn I major lines at 303.4115 nm, 317.5035 nm, 326.2331 nm, 380.1011 nm, 452.4734 nm, 563.1676 nm, and 606.9117 nm, and Sn II lines located at 335.1952 nm, 558.8815 nm, 579.886 nm, 645.3542 nm, 684.4186 nm, and 774.1425 nm. As seen, the dominance of tin spectral lines with no pre-eminent impurity signals validates that the powder of SnO_2 is extremely pure.

Thin films were deposited with high-purity SnO_2 powder by PLD with deposition done at room temperature (RT) under vacuum, and the film thickness was measured by the optical interferometric method, which was measured at approximately 200 nm. X-ray diffraction (XRD) assessment of film crystallinity is

depicted in Fig. (3). The profile shows intense and defined peaks corresponding to the tetragonal rutile phase of SnO_2 (JCPDS card no. 96-900-9083), thus confirming the phase purity of the deposited films [19]. The strongest observed diffraction value occurs at $2\theta \approx 26.45°$ assigned to the (110) crystallographic plane, reflecting a strong corresponding preference to move along this direction. This preferred (110) orientation is typically favorable for electron transport in thin films of SnO_2, with the crystalline quality, and carrier scattering is reduced; thus, SnO_2 is a suitable window and interface layer material of photovoltaic devices. The structural parameters obtained using the XRD are summarized in table (1), in good agreement with the standard values. Calculated crystallite sizes range from 26.7 to 46.5 nm, which supports the nanocrystalline behavior of these SnO_2 films. Extremely low defect density and high crystallinity are indicated by the narrow FWHM and high peak intensities. At the experimental and standard level, d-spacing values show minor deviations, indicating slight lattice distortion. Thus, it was found that the lattice parameters of the tetragonal SnO_2 are a = 4.7605 Å and c = 3.1965 Å, which suggests low tensile strain within the films. The slight strain can be explained by PLD growth at room temperature, as limited surface diffusion may promote slight non-stoichiometry and oxygen-vacancy-related lattice distortion under vacuum conditions [20].

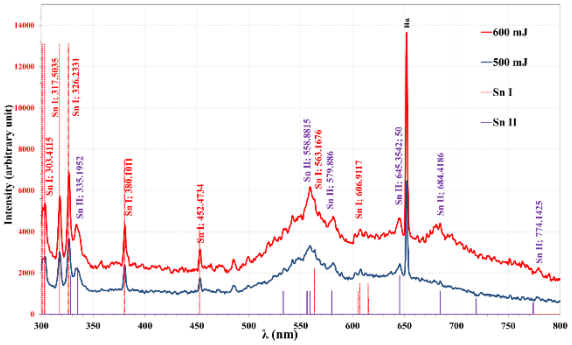

Fig. (2) LIBS emission spectrum of SnO_2 powder

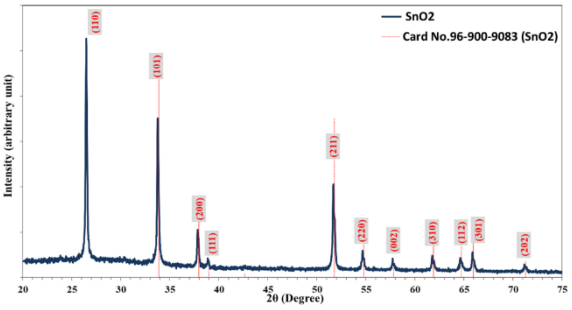

Fig. (3) XRD pattern for SnO_2 thin films at room temperature

AFM analysis showed a smooth and homogeneous surface morphology with low RMS roughness of 3.64 nm, indicating that SnO_2 thin films possess high surface quality. This low roughness is advantageous in minimizing optical scattering losses and ensuring intimate interfacial contact with porous silicon, which is essential for efficient charge collection and reduced recombination in solar cell devices [21]. The observed larger grain size (64.06 nm) than the crystallite size obtained from XRD reflects the aggregation of several crystallites into single surface grains, which is common in the case of PLD-grown films [22].

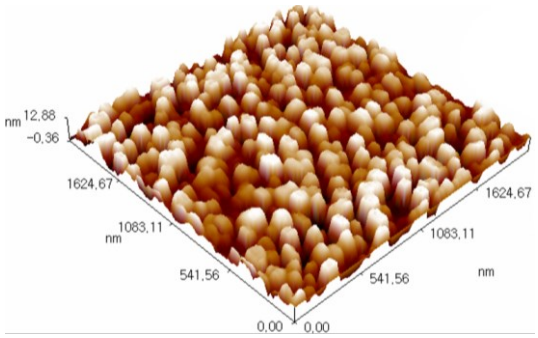

Fig. (4) 3D AFM image for SnO_2 thin films at room temperature

Figures (5) and (6) display the optical properties of SnO_2 thin films deposited by the PLD method, based on absorbance, transmittance, and optical bandgap. Intrinsic electronic transitions and defect states determine the UV absorption of these films, whereas the transparency of the films in the visible region shows little effect.

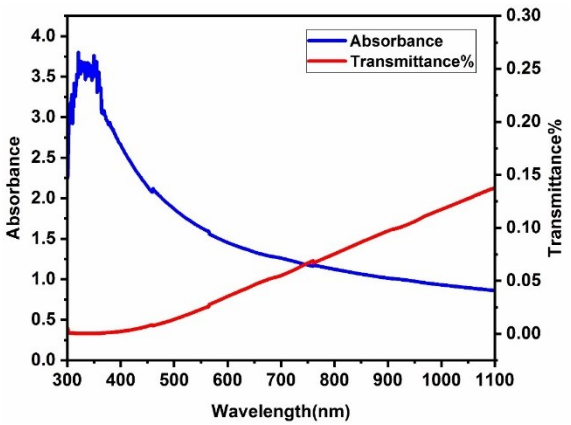

Fig. (5) Absorbance and transmittance of SnO_2 thin film at room temperature

Transmittance spectra have high transmittance at wavelengths longer than 400 nm, with visible transmittance reaching approximately 90%. This is consistent with reference [23]. The high optical transmittance implies that SnO_2 thin films are a suitable transparent window and interfacial layer, wherein the visible light enters the porous silicon absorber layer of the solar cell structure [24].

The Tauc's method with a direct allowed transition was employed to calculate the optical bandgap. Extrapolation over the linear region close to the absorption edge generates an optical bandgap of

approximately 3.4 eV, which is characteristic of wide-bandgap SnO_2 thin films and consistent with previously reported values [25]. The marginally lower bandgap as compared to bulk SnO_2 can be associated with defect-related states and room-temperature growth conditions.

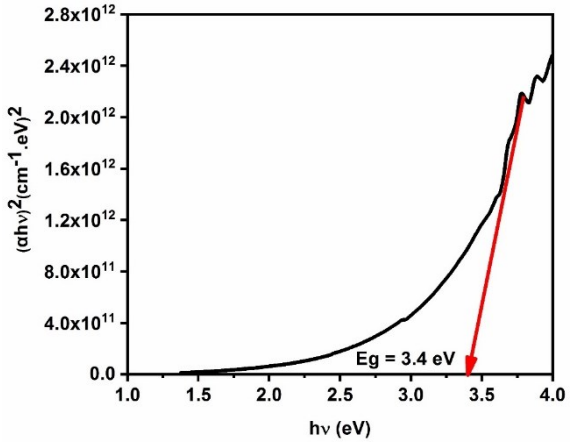

Fig. (6) Determination of energy band gap for SnO_2 thin films at room temperature

Figure (7) depicts the J–V characteristics of the SnO_2/PSi solar cell under illumination, where current density (J) is plotted as a function of the applied voltage (V). With an incident power density of P_{in}=100 mW/cm², the device has a short-circuit current density of about 29 mA/cm² and an open-circuit voltage of approximately 0.4 V. The comparatively large J_{SC} reveals effective light harvesting by the porous silicon substrate and a favorable optical coupling at the SnO_2/PSi interface.

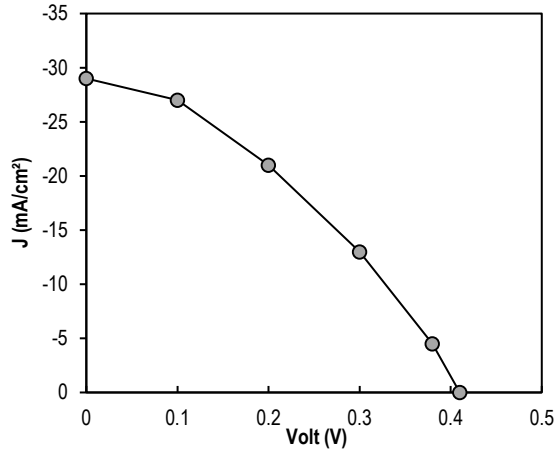

Fig. (7) J-V characteristic for SnO_2/PSi structure

The nearly linear J–V response in the absence of a significant knee yields a low fill factor of 0.325 and a conversion efficiency of 3.77%. This behavior means that device performance is primarily limited by electrical losses, such as series resistance and interfacial recombination at the SnO_2/PSi junction, rather than insufficient crystallinity, surface smoothness, or optical transparency of the SnO_2 films. The room-temperature deposition and lack of post-deposition electrical optimization may contribute to these losses.

To situate the current results in a broader context, a comparison with representative studies reported in the literature is provided. Table (2) lists the selected structural, optical, and photovoltaic parameters of SnO_2-based thin films formed with different deposition methods. The objective of this comparison is to demonstrate the relative importance of the realized film smoothness, optical bandgap, and device performance against previously reported SnO_2 and tin-oxide-based systems, as well as to elucidate the similarities and differences attributed to deposition conditions and material configurations.

4. Conclusion

SnO_2 thin films prepared in this work using PLD show good optical properties, and high crystallinity, and would allow for increased efficiency of solar cells. These properties will, in the future, be optimized even further. This will provide the opportunity to keep improving the overall parameters of solar cell performance with even higher efficiencies.

References

[1] M.A. Issa and K.A. Aadim, "Optical and structural characterization of ZnO:NiO nanocomposite prepared by pulsed laser deposition method", *J. Opt.*, 54 (2025) 2357-2362.

[2] B.A. Hasan and A.A. Hasan, "Effect of antimony oxide additive on characteristics of $(SnO_2)_{1-x}(Sb_2O_3)_x$ composite thin films synthesized by pulsed-laser deposition", *Iraqi J. Appl. Phys.*, 21(3) (2025) 355-364.

[3] M.A. Issa and K.A. Aadim, "Study the structural and optical properties of zinc oxide prepared by pulse laser deposition", *J. Opt.*, (2024), doi: 10.1007/s12596-024-02034-2.

[4] H. Yuan et al., "Development of laser-ablated aluminum plasma plume during the irradiation of laser pulse", *J. Laser Appl.*, 36(1) (2024) 012031.

[5] M.A. Issa and K.A. Aadim, "Influence of laser energy on structural and optical properties of $ZnO_{(x)}$:$NiO_{(1-x)}$ films prepared by pulse laser deposition", *J. Opt.*, (2024), doi: 10.1007/s12596-024-02212-2.

[6] B. Tiss et al., "Growth of Al: ZnO nano-flowers by pulsed laser ablation deposition", *Opt. Laser Technol.*, 174 (2024) 110673.

[7] M.A. Essa and K.A. Aadim, "Spectroscopic studying of plasma parameters for SnO_2-doped ZnO prepared by pulse Nd:YAG laser deposition", *Iraqi J. Phys.*, 17(42) (2019) 125-135.

[8] J. Bae and H. Jeon, "Effects of deposition and annealing temperature on atomic layer-deposited

tin dioxide thin films", *J. Korean Phys. Soc.*, 87 (2025) 186–193.
[9] Z. Chen et al., "Analysis of the effect of graphene, metal and metal-oxide transparent electrodes on the performance of organic optoelectronic devices", *Nanomaterials*, 13(1) (2022) 25.
[10] X. Chen et al., "Enhanced light transmittance of electron transport layer through bilayer SnO_2 for high-performance semitransparent perovskite solar cells", *ChemSusChem*, 18(11) (2025) e202402582.
[11] G. Kulesza-Matlak et al., "Deposition of SnO_2 as a functional layer on a porous silicon substrate for potential tandem solar cell application", *Opto-Electron. Rev.*, 33(1) (2025) e152685.
[12] Z. Kenzhaev et al., "The physical mechanisms of gettering properties of nickel clusters in silicon solar cells", *Phys. Sci. Technol.*, 11(1-2) (2024) 13-22.
[13] E.S. Hassan et al., "Physical properties of indium-doped cadmium sulfide thin films prepared by SPT", *J. Phys.: Conf. Ser.*, 1294(2) (2019) 022008.
[14] M.O. Dawood et al., "Effect of Li doping on structure and optical properties of NiO nano thin films by SPT", *AIP Conf. Proc.*, 2213(1) (2020) 020102.
[15] X. Zheng, J. Li and Y. Zhou, "X-ray diffraction measurement of residual stress in PZT thin films prepared by pulsed laser deposition", *Acta Materialia*, 52(11) (2004) 3313-3322.
[16] P. Bhavya et al., "Effect of viscosity and dielectric constant variation on fractional fluorescence quenching analysis of coumarin dye in binary solvent mixtures", *Luminescence*, 33(5) (2018) 933-940.
[17] M. Hafez and S. Taha, "Exploration of structural and optical properties of diphenyl carbazide thin films for optoelectronic application", *J. Mol. Struct.*, 1325 (2025) 141032.
[18] P.H. Andrade et al., "Band gap analysis in MOF materials: Distinguishing direct and indirect transitions using UV–vis spectroscopy", *Appl. Mater. Today*, 37 2024) 102094.
[19] R. Shen et al., "Flower-like tin oxide membranes with robust three-dimensional channels for efficient removal of iron ions from hydrogen peroxide", *Chin. J. Chem. Eng.*, 65 (2024) 1-7.
[20] A. Herklotz et al., "Strain coupling of oxygen non-stoichiometry in perovskite thin films", *J. Phys.: Cond. Matter*, 29(49) (2017) 493001.
[21] V.P. Hoang Huy and C.W. Bark, "Review on surface modification of SnO_2 electron transport layer for high-efficiency perovskite solar cells", *Appl. Sci.*, 13(19) (2023) 10715.
[22] M. Sharma et al., "Investigation of local geometrical structure, electronic state and magnetic properties of PLD grown Ni doped SnO_2 thin films", *J. Electron. Spectro. Relat. Phenom.*, 232 (2019) 21-28.
[23] P. Chetri and A. Choudhury, "Investigation of optical properties of SnO_2 nanoparticles", *Physica E*, 47 (2013) 257-263.
[24] A.E. Delahoy and S. Guo, "Transparent conducting oxides for photovoltaics," in **Handbook of Photovoltaic Science and Engineering**, 2nd ed., (2011), pp. 716-796.
[25] C. Guillén, "Determination of the band gap energy of SnO_2 and ZnO thin films with different crystalline qualities and doping levels", *Electron. Mater.*, 6(1) (2025) 3.
[26] S.A. Fadaam et al., "Synthesis and characterization of metastable phases of SnO and Sn_3O_4 thin films for solar cells applications", *J. Phys.: Conf. Ser.*, 1963(1) (2021) 012003.
[27] L.K. Ibraheem and B.A. Hasan, "Role of tin oxide on the structural, optical and electrical properties of pulsed laser deposited $(ZnO)_{1-x}(SnO_2)_x$ composite thin films", *Iraqi J. Phys.*, 23(3) (2025) 50-65.
[28] H.A.K. Hmoud, "Study of structural morphology and optical properties of nickel doped nanostructured tin oxide thin films", *Mustansiriyah J. Sci. Educ.*, 23(1) (2022) 29-38.
[29] A.K. Abass and S.A. Abd Al-Hassan, "Preparation of composite thin films of tin oxide with cobalt oxide and study their structure and optical characteristics", *Al-Qadisiyah J. Pure Sci.*, 24(2) (2019) 36-41.
[30] A.R. Safah, Z.N. Majeed and K.H. Mohmood, "Influence of the zinc tin oxide nanoparticle proportions on the optical properties prepared by the laser method", *Tikrit J. Pure Sci.*, 25(6) (2020) 88-95.

Table (1) XRD peaks for SnO_2 thin films prepared by PLD

Sample	2θ (Deg.)	FWHM (Deg.)	d_{hkl} Exp.(Å)	d_{hkl} Std.(Å)	G.S (nm)	hkl	Strain	Phase
SnO_2	26.4568	0.1757	3.3662	3.3498	46.5	-110	0.00489581	Tet.SnO_2
	33.7482	0.2196	2.6537	2.6439	37.8	-101	0.00370665	Tet.SnO_2
	37.8331	0.2636	2.3761	2.3686	31.9	-200	0.00316643	Tet.SnO_2
	38.8873	0.2635	2.314	2.3087	32	-111	0.00229566	Tet.SnO_2
	51.6691	0.3074	1.7677	1.7642	28.7	-211	0.0019839	Tet.SnO_2
	54.6559	0.3074	1.6779	1.6749	29.1	-220	0.00179115	Tet.SnO_2
	57.7306	0.3074	1.5956	1.5932	29.5	002	0.0015064	Tet.SnO_2
	61.7716	0.2636	1.5006	1.4981	35.1	-130	0.00166878	Tet.SnO_2
	64.6706	0.3514	1.4402	1.4388	26.8	-112	0.00097303	Tet.SnO_2
	65.8565	0.3514	1.4171	1.4149	26.9	-301	0.00155488	Tet.SnO_2
	71.1713	0.2635	1.3237	1.322	37.1	-202	0.00128593	Tet.SnO_2
	78.6384	0.3075	1.2157	1.2147	33.4	-321	0.00082325	Tet.SnO_2

Table (2) compares the present results with representative SnO_2-based thin films reported in the literature

Work	Material System	Deposition Technique	Substrate Temp.	E_g (eV)	RMS Roughness (nm)	Photovoltaic Performance	Ref.
This work	SnO_2 / PSi	PLD	RT	3.4	3.64	Jsc = 29 mA/cm² FF = 32.5% η = 3.77%	—
Fadaam et al.	SnO / Sn_3O_4	Thermal evaporation + oxidation	150–550 °C	3.1–2.4	—	η = 2–5.1%	[26]
Ibraheem et al.	$(ZnO)_{1-x}(SnO_2)_x$	PLD	R.T	3.4	—	No solar cell	[27]
Hmoud	SnO_2:Ni	CSP	—	3.68–3.58	6.78–3.16	No solar cell	[28]
Abass et al.	SnO_2:Co	CSP	400 °C	4.5-2.5eV.	—	No solar cell	[29]
Safah et al.	ZnO/SnO_2 mixed	PLD	Annealed	3.2–3.3	—	No solar cell	[30]

